

Icosahedral Crown Gold Nanocluster $\text{Au}_{43}\text{Cu}_{12}$ with High Catalytic Activity

Yi Gao, Nan Shao, Yong Pei, and Xiao Cheng Zeng*

Department of Chemistry and Nebraska Center for Nanoscience and Materials, University of Nebraska-Lincoln, Lincoln, Nebraska, 68588

ABSTRACT Structural and catalytic properties of the gold alloy nanocluster $\text{Au}_{43}\text{Cu}_{12}$ are investigated using a density-functional method. In contrast to the pure Au_{55} nanocluster, which exhibits a low-symmetry C_1 structure, the 55-atom “crown gold” nanocluster exhibits a multishell structure, denoted by $\text{Au}@\text{Cu}_{12}@\text{Au}_{42}$, with the highest icosahedral group-symmetry. In addition, density functional calculations suggest that this geometric magic-number nanocluster possesses comparable catalytic capability as a small-sized Au_{10} cluster for the CO oxidation, due in part to their low-coordinated Au atoms on vertexes. The gold alloy nanocluster also shows higher selectivity for styrene oxidation than the bare $\text{Au}(111)$ surface.

KEYWORDS Crown gold, magic-number cluster, gold catalysis, selectivity, density-functional theory

Gold nanoparticles (AuNPs) possess unusual catalytic capability.^{1–13} For example, supported AuNPs can oxidize CO into CO_2 well below the room temperature.⁷ Previous studies have shown that catalytic efficiency of gold nanostructures can be affected by a number of factors, which include the dimensionality, morphology, fluxionality, and electronic states of the nanostructures, as well as the type and surface structures of the supports. To date, most theoretical studies of catalytic activities of gold nanoclusters, either supported or unsupported, have been focused on subnanometer gold clusters Au_N ($N \leq 20$),¹⁴ whereas most experimental studies have been focused on catalytic activities of AuNPs with sizes typically much larger than 1 nm. Recently, Turner et al. investigated catalytic activities of AuNPs in the size range 1.4–30 nm.¹⁵ They found that the 55-atom gold nanoclusters (~ 1.4 nm in length scale) exhibit highest catalytic activity toward selective oxidation of styrene, even on inert supports.¹⁵

Besides pure gold nanoclusters, gold alloy clusters have also attracted growing attention owing to their tunable properties through mixing the second metal element.¹⁶ For example, the endohedral gold cluster $\text{W}@\text{Au}_{12}$, first predicted by Pyykkö and Runeberg,¹⁷ was proven to possess the icosahedral symmetry and a large gap between the highest occupied molecular orbital and the lowest unoccupied molecular orbital (HOMO–LUMO gap). This geometric and electronic “magic-number” gold alloy cluster was later detected by Wang et al. using photoelectron spectroscopy.^{18,19} Molina and Hammer found that a Na-doped Au_{20} cluster is more active than the bare pyramidal Au_{20} cluster based on density functional theory (DFT) calculations.²⁰ Walter and Häkkinen studied properties of a mixed gold

cluster SiAu_{16} that has 20 valence electrons.²¹ A series of mixed gold clusters $\text{M}@\text{Au}_n$ ($n = 9–17$, M = Pd, ...Na–K),²² all having 18 valence electrons, were also studied, and some of these clusters were predicted to show high catalytic activities.²³ Structural evolution of small-sized Cu-doped gold clusters $\text{Au}_{n-1}\text{Cu}^-$ ($n = 13–19$) was investigated by Zorriatein et al.²⁴ Au–Cu, Au–Ni, and Au–Co alloy clusters with size up to 38 atoms were also studied by Ferrando et al.²⁵ Experimentally, Wang et al. demonstrated stability of a number of endohedral gold-cage clusters, including $\text{M}@\text{Au}_{16}^-$ (M = Cu, Ag, In, Zn, Fe, Co, Ni) and $\text{Cu}@\text{Au}_{17}^-$ by anion photoelectron spectroscopy.²⁶

For larger size of gold alloy clusters, we are aware of a previous theoretical study of 55-atom clusters by Chang et al.²⁷ They predicted that $\text{Au}_{25}\text{Ag}_{30}$ can be a more effective catalyst than pure Au_{55} or Ag_{55} cluster. Moreover, they showed by using a semiempirical method^{28,29} that both Au_{54}Cu and $\text{Au}_{43}\text{Cu}_{12}$ gold alloy clusters are likely to exhibit the icosahedral structure. It is known that for pure 55-atom coinage clusters, only the bare Ag_{55} and Cu_{55} exhibit the icosahedral structure, whereas the bare Au_{55} cluster has a low-symmetry C_1 structure.^{30–33} Hence, it would be interesting to see the extent to which a binary gold alloy cluster can be converted from C_1 to icosahedral structure through atom-by-atom substitution. Clusters that have the icosahedral structure (such as $\text{W}@\text{Au}_{12}$, Cu_{55} , and Ag_{55}) are generally called “geometric magic-number” clusters. For many metal or metal alloy clusters, icosahedral clusters tend to be more stable than low-symmetry counterparts and may possess special properties. For example, Wang et al. recently predicted that the icosahedral gold alloy cluster $\text{Mn}_{13}@\text{Au}_{20}^-$ can possess a very large magnetic moment.³⁴ Icosahedral metal clusters may also have special catalytic properties because they have more low-coordinated atomic sites than other low-symmetry isomers. It is also known that low-coordinated Au atoms are more likely to be the active sites

* To whom correspondence should be addressed. E-mail: xceng@phase2.unl.edu.

Received for review: 01/4/2010

Published on Web: 02/15/2010

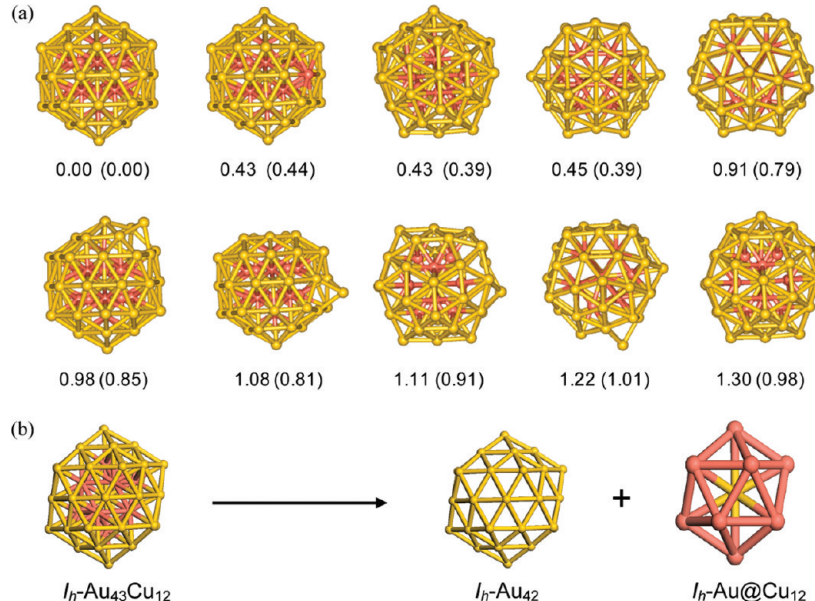


FIGURE 1. (a) Structures of 10 lowest-lying isomers of $\text{Au}_{43}\text{Cu}_{12}^-$ cluster and relative energies ΔE (in unit of eV), based on the KT2/TZP calculation (PBE/DNP results in parentheses), with respect to the lowest-energy isomer. Except isomer 2, all isomers contain a 13-atom core consisting of 12 Cu atoms and 1 Au atom. Isomer 2 has 1 Cu atom on the shell, but still a 13-atom core consisting of 11 Cu atoms and 2 Au atoms. (b) The gold shell and copper–gold core of the lowest-energy isomer of $I_h\text{-Au}@\text{Cu}_{12}@\text{Au}_{42}^-$. Color code: red (Cu), gold (Au).

for catalytic reaction than high-coordinated atoms.^{14c} Hence, a search for the 55-atom gold alloy cluster with the icosahedral symmetry would be useful for undertaking a comparative study of structure–activity relationship for isomers with different structures. To this end, we recently studied doping a single metal atom to the Au_{55}^- cluster. We found that a single-atom dopant is unlikely to convert the low-symmetry parent structure to the icosahedral (I_h) structure. For example, the gold–aluminum cluster $\text{Al}@\text{Au}_{54}^-$, even with shell-closing 58-valence electrons, still prefers a low-symmetry C_1 structure over the I_h structure.³⁵ Therefore, we expect more substituting dopant atoms are needed to convert the low-symmetry Au_{55}^- structure to the icosahedral structure.

In this letter, we report a 55-atom multishell gold alloy cluster, $\text{Au}@\text{Cu}_{12}@\text{Au}_{42}$, which not only has the icosahedral structure in the ground state, but also possesses promising catalytic activities for CO oxidation, and selectivity for styrene oxidation. Because this gold alloy cluster has 91.7 % of Au and 8.3 % of Cu in weight, the weight percentage of gold is equivalent to that of the “crown gold” (22 kt. = 91.7 wt %), a composition formula widely used in jewelry industry since the Victorian era.

The first-principles calculations were carried out using a density functional theory (DFT) method within the generalized-gradient approximation in the form of the Perdew–Burke–Ernzerhof (PBE) functional.³⁶ Semicore pseudopotential was opted along with the double numerical plus polarization (DNP) basis set for geometric optimization.³⁷ Catalytic activities of the nanocluster were assessed based on two chemical reactions, (1) the CO oxidation and (2) styrene epoxidation. The reaction pathways were computed using the nudged elastic band (NEB) method.³⁸ All computa-

tions were performed by using the DMol3 software package.³⁷ To search for the lowest-energy structure of the 55-atom Au–Cu alloy cluster, we employed the basin-hopping global-optimization method coupled with the DFT geometry optimization.^{39,40} More than 100 low-energy isomers were collected.

To examine relative stabilities among top-10 low-lying isomers, we also computed relative energies of the 10 lowest-lying isomers based on the KT2 functional⁴¹ with a larger TZP (triple- ζ 1 polarization function) basis set (see Supporting InformationTable S1). Recently, Aikens showed that the KT2 functional is one of very accurate functionals for computing structural and electronic properties of the $\text{Au}_{25}(\text{SCH}_3)_{18}$ cluster, compared to the experiment.⁴² As a benchmark test of the KT2/TZP level of theory, we examined relative stability of two low-lying isomers of Au_{12}^- , one planar isomer and one three-dimensional (3D) isomer (see Supporting InformationFigure S1). We found that the 3D isomer is 0.37 eV lower in energy than the planar isomer, consistent with experiments^{43,44} and other benchmark tests based on the M06-L and M06 functionals.⁴⁵ Thus, the KT2/TZP level of theory would be qualitatively more accurate than the PBE/TZP level in predicting energy ranking among low-lying isomers of $\text{Au}_{43}\text{Cu}_{12}^-$ cluster. The KT2/TZP calculations were performed using the ADF software package.⁴⁶ Since the KT2/TZP calculations are much more demanding computationally than the PBE/DNP calculations, we only used this level of theory to confirm the lowest-energy isomer (Figure 1), and our studies of catalytic properties of $\text{Au}_{43}\text{Cu}_{12}^-$ cluster were entirely based on the PBE/DNP level of theory.

As shown in Figure 1, the predicted lowest-energy isomer of $\text{Au}_{43}\text{Cu}_{12}^-$ exhibits an icosahedral multishell structure

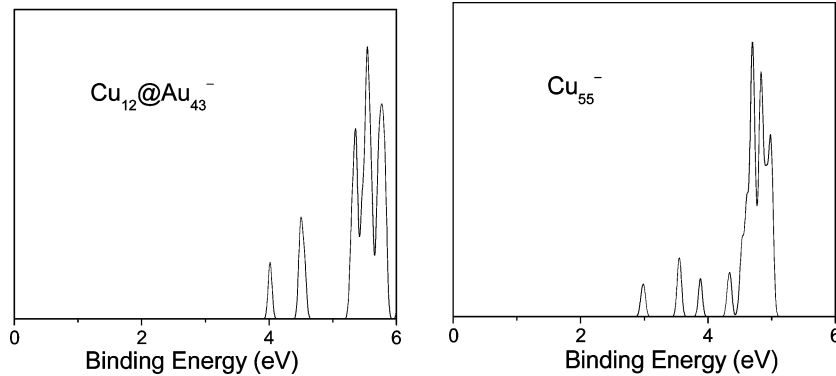


FIGURE 2. Simulated anion photoelectron spectra of $\text{Au}@\text{Cu}_{12}@\text{Au}_{42}^-$ and Cu_{55}^- using the PBE/PBE/LANL2DZ level of theory implemented in Gaussian 03 program.⁵⁰

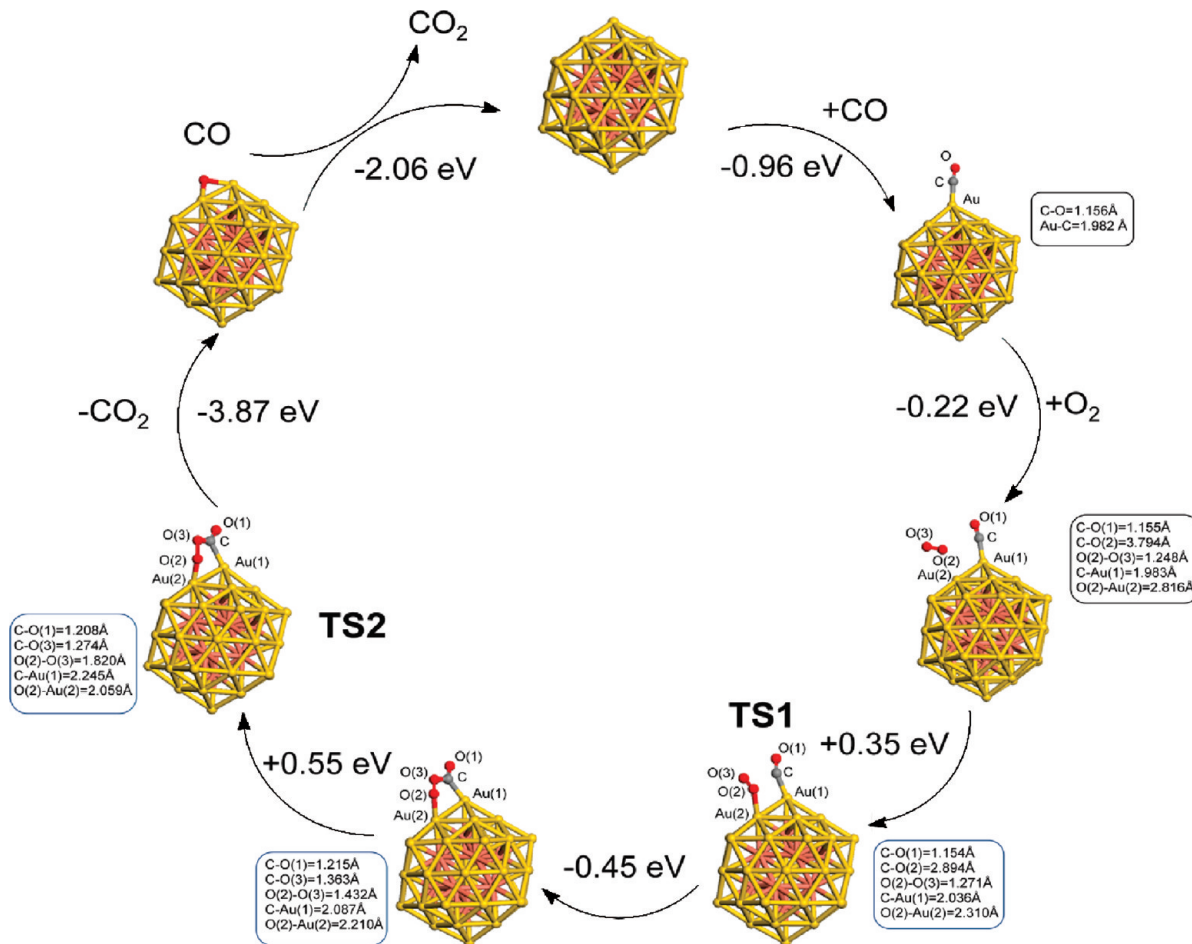


FIGURE 3. Catalytic cycle of $2\text{CO} + \text{O}_2 \rightarrow 2\text{CO}_2$ reaction on the anion cluster $I_h\text{-Au}@\text{Cu}_{12}@\text{Au}_{42}^-$. Calculation is done at the PBE/DNP level of theory. TS1 and TS2 denote the first and second transition state, respectively.

$\text{Au}@\text{Cu}_{12}@\text{Au}_{42}^-$ where the 12 copper atoms encompass a gold atom to form an icosahedral (I_h) core. Apparently, the $I_h\text{-Au}@\text{Cu}_{12}$ core is sufficiently robust to enforce the icosahedral symmetry for the Au_{42} shell. For the 10 lowest-lying isomers shown in Figure 1a, the lowest-energy $I_h\text{-Au}@\text{Cu}_{12}@\text{Au}_{42}^-$ isomer is 0.43 eV lower in energy than the second and third low-lying isomers and is appreciably lower in energy than all other seven isomers. Among the 10 lowest-

lying isomers, all but the isomer 2 possess a 13-atom core consisting of 12 Cu atoms and 1 Au atom. The isomer 2 has one Cu atom in the shell, but still has a 13-atom core consisting of 11 Cu atoms and 2 Au atoms. To our knowledge, this global search provides the first DFT calculation evidence that a 55-atom crown-gold cluster has the icosahedral symmetry in the ground state. The bond lengths of Au–Au in $I_h\text{-Au}@\text{Cu}_{12}@\text{Au}_{42}^-$ isomer range from 2.828 to

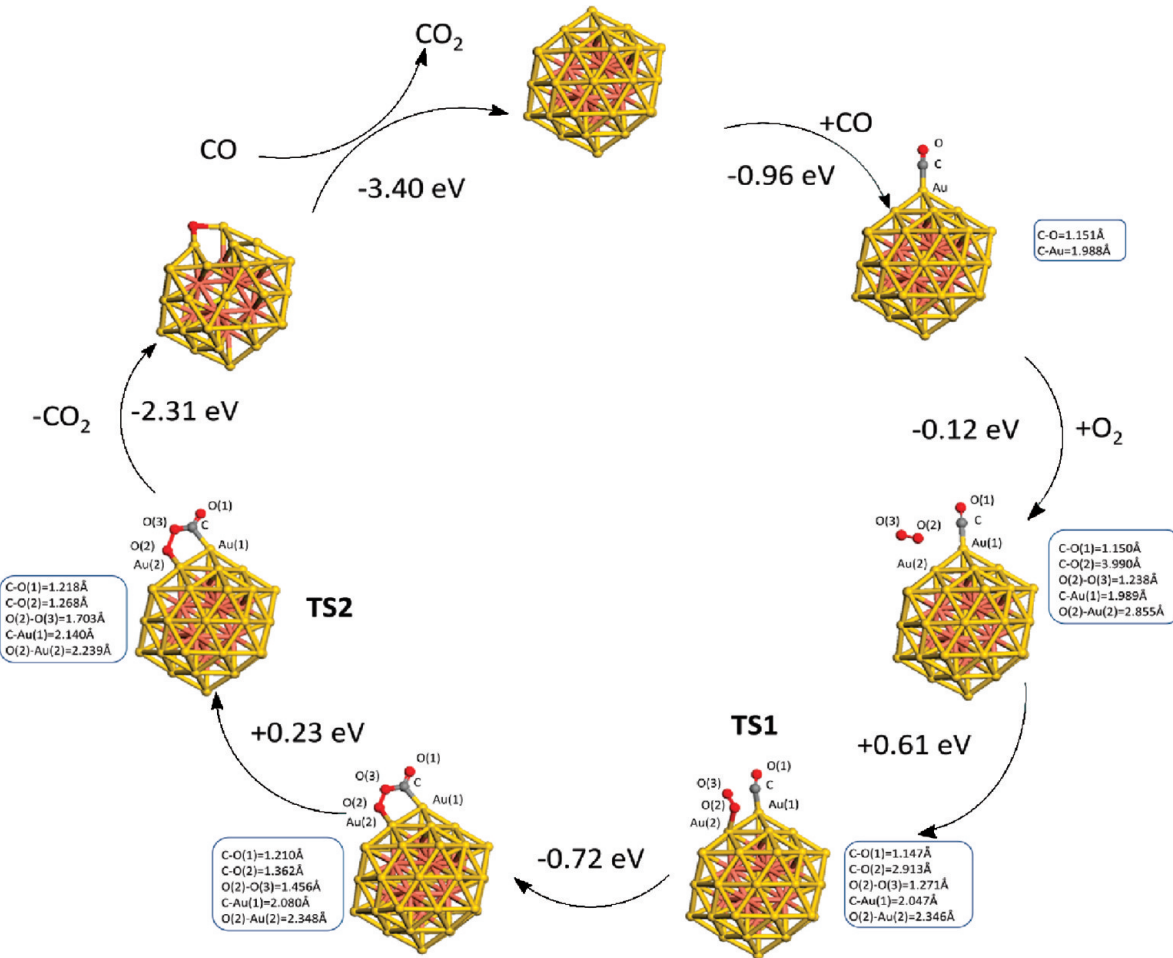


FIGURE 4. Catalytic cycle of $2\text{CO} + \text{O}_2 \rightarrow 2\text{CO}_2$ on the neutral cluster $I_h\text{-Au@Cu}_{12}\text{@Au}_{42}$. Calculation is done at the PBE/DNP level of theory.

2.892 Å, and those of Cu–Cu are 2.772 Å. The Au–Au bond lengths are comparable to those in the known “magic-number” gold alloy clusters, for example, $I_h\text{-W@Au}_{12}$ ¹⁷ and $D_{2d}\text{-Zr@Au}_{14}$.²² The Cu–Cu bond lengths are longer than those in bulk copper and pure copper clusters (typically ~2.55 Å),^{47,48} which may be due to stronger interaction with gold. In addition, the bond lengths of Au–Cu are 2.630 Å (inner shell, center Au to vertex Cu), 2.745 Å (outer-shell, vertex Au to vertex Cu) and 2.807 Å (outer-shell, bridge Au to vertex Cu). The shorter Au–Cu bond lengths in the inner core reflect the higher cohesivity of the Au@Cu₁₂ core. The Hirshfeld charge analysis shows that all Au atoms exhibit negative charges while all Cu atoms exhibit positive charges (Cu, 0.039 e/each). Moreover, the Au atom at the center exhibits the most negative charge (−0.059 e). Hence, the inner Au@Cu₁₂ core has a net charge of 1.41 e while the Au₄₂ outer shell has a net charge of −1.41 e, indicating that the encapsulation of 12 Cu atoms as a middle shell results in the Au₄₂ outer shell more negatively charged. The lowest harmonic vibrational frequency of $I_h\text{-Au@Cu}_{12}\text{@Au}_{42}^-$ is 31.6 cm^{−1}, comparable to 31.5 cm^{−1} of $I_h\text{-W@Au}_{12}$ ¹⁷ and 29.2 cm^{−1} of $T_d\text{-Au}_{20}$.⁴⁹

We also studied properties of the “neutral” multishell cluster Au@Cu₁₂@Au₄₂ with the icosahedral symmetry. The bond lengths of Au–Au, Au–Cu, and Cu–Cu for the neutral cluster $I_h\text{-Au@Cu}_{12}\text{@Au}_{42}$ are 2.832–2.886, 2.630–2.805, and 2.766 Å, respectively, indicating that the geometry of neutral species is almost unchanged with one electron being removed from the anionic counterpart. Moreover, the lowest harmonic vibrational frequency of $I_h\text{-Au@Cu}_{12}\text{@Au}_{42}$ is 32.1 cm^{−1}, very close to that of the anionic counterpart. The Hirshfeld charge analysis shows that the charge distribution in the inner core is very close to that in the anionic counterpart (Cu, 0.0396 e/each; core Au, −0.060 e). As a result, the inner core of Au@Cu₁₂ exhibits 0.415 e while the outer shell exhibits −0.415 e. It appears that the Au@Cu₁₂ inner core is somehow shielded by the outer shell so that adding extra negative charges would only affect the charges on the outer shell. We also computed the embedding energy of the $I_h\text{-Au@Cu}_{12}$ core within the Au₄₂ shell, defined as ΔE [embedding] = ΔE [Au@Cu₁₂@Au₄₂] − ΔE [Au@Cu₁₂] − ΔE [Au₄₂], which is −22.5 eV. The average binding energy per atom for $I_h\text{-Au@Cu}_{12}\text{@Au}_{42}$ is 2.70 eV, stronger than that (2.48 eV/atom) of the magic-number gold alloy cluster

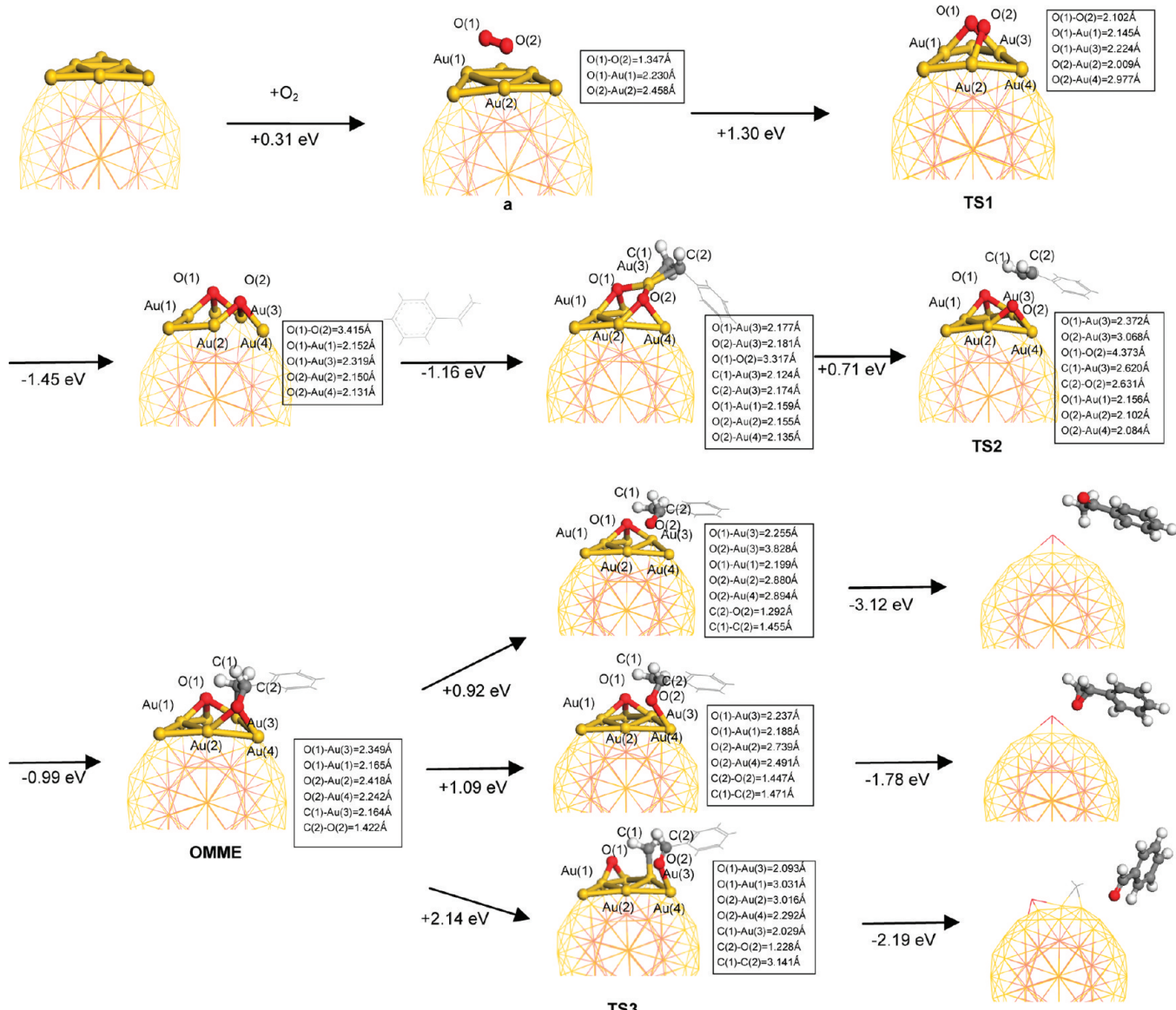


FIGURE 5. A catalytic reaction pathway for the styrene selective oxidation on the anion cluster $I_h\text{-Au@Cu}_{12}\text{@Au}_{42}^-$. A typical active site on a Au_6 triangle is shown. Calculation is done at the PBE/DNP level of theory.

$I_h\text{-W@Au}_{12}$. Note also that the average binding energy per atom for the Au_{42} outer-shell and Cu_{12} middle shell is 2.37 and 1.93 eV/atom, respectively. Both values are smaller than the binding energy of the alloy cluster, confirming that the Au-Cu interaction is stronger than Au-Au and Cu-Cu interactions, hence, the high stability of the alloy cluster $I_h\text{-Au@Cu}_{12}\text{@Au}_{42}$.

In Figure 2, we plot the simulated anion photoelectron spectra of $I_h\text{-Au@Cu}_{12}\text{@Au}_{42}^-$ and $I_h\text{-Cu}_{55}^-$. Interestingly, the computed first vertical detachment energy (VDE) of $I_h\text{-Au@Cu}_{12}\text{@Au}_{42}^-$ (3.99 eV) is significantly greater than the measured value of 2.96 eV for $I_h\text{-Cu}_{55}^-$,³⁰ but smaller than the measured value of ~4.7 eV for Au_{55}^- .^{30,31} The difference in VDE appears to be correlated with the number of Au atoms in the clusters, namely, less Cu atoms in the gold alloy cluster give rise to higher VDE.

As mentioned previously, Turner et al. reported that both ligand-covered $\text{Au}_{55}(\text{PPh}_3)_{12}\text{Cl}_6$ and bare Au_{55} nanoparticles show remarkable catalytic activity, as evident by their direct oxidation of styrene with O_2 to form benzaldehyde, styrene epoxide, and acetophenone.¹⁵ They found that the gold nanoclusters exhibit a sharp size-threshold in catalytic activity. Among them, the Au_{55} cluster with size ~1.4 nm shows the highest catalytic activity as well as high selectivity for the styrene oxidation due to overwhelmingly high yield of benzaldehyde, compared to the yield of benzoic acid or styrene epoxide. It is worth noting again that the bare Au_{55} cluster has a low-symmetry structure^{30,31} whereas the $\text{Au}_{55}(\text{PPh}_3)_{12}\text{Cl}_6$ cluster is likely to have the icosahedral symmetry.⁵¹ Although the $\text{Au}_{55}(\text{PPh}_3)_{12}\text{Cl}_6$ cluster is partially covered by the ligands, it still shows reasonably high catalytic activities due to the existence of 24 open low-coordinated

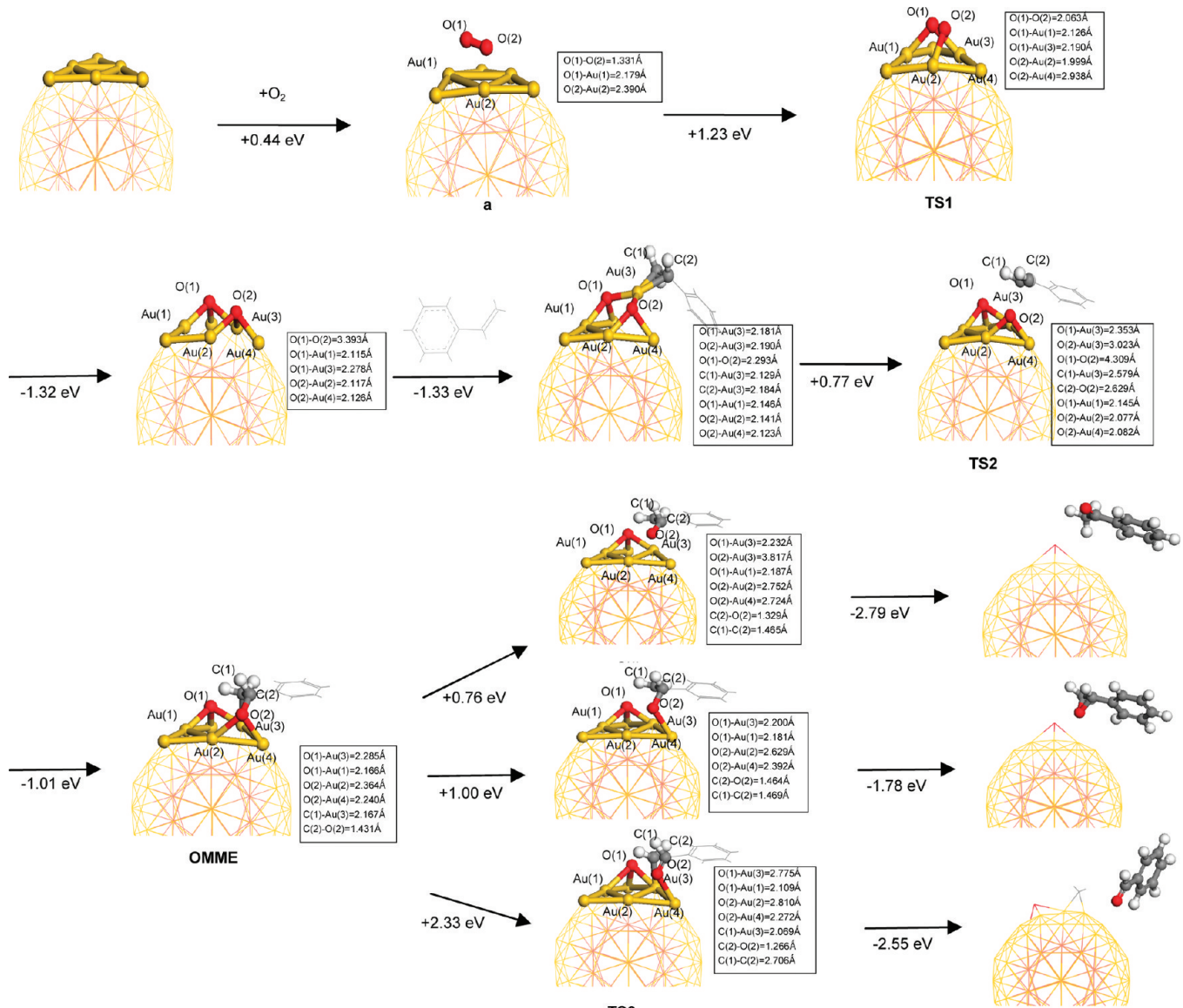


FIGURE 6. A catalytic reaction pathway of the styrene selective oxidation on the neutral cluster $I_h\text{-Au@Cu}_{12}\text{@Au}_{42}$. A typical active site on a Au_6 triangle is shown. Calculation is done at the PBE/DNP level of theory.

Au sites on the surface of Au_{55} . The important role of low-coordinated Au atoms in the catalytic reactions has been discussed in many previous studies.^{14,23,52,53} Therefore, an assessment of catalytic activities of the crown-gold cluster $I_h\text{-Au@Cu}_{12}\text{@Au}_{42}$ will be of scientific interest to seek more efficient gold alloy nanocatalysts. To this end, we considered two fundamental reactions as benchmark probes for the evaluation of catalytic activities, (1) the CO oxidation and (2) styrene epoxidation.

The catalytic reaction pathways for the CO oxidation on the anion and neutral cluster $I_h\text{-Au@Cu}_{12}\text{@Au}_{42}$ are displayed in Figures 3 and 4, respectively. As shown in Figure 3, the CO and O_2 molecules can be favorably coadsorbed on two neighboring low-coordinated Au atoms on the $I_h\text{-Au@Cu}_{12}\text{@Au}_{42}^-$ cluster with coadsorption energy of CO_2 and O_2 about -1.18 eV . This adsorption energy (1.18

eV) for the $\text{CO} + \text{O}_2$ species is stronger than that on a model bare Au_{10} cluster ($\sim 0.7 \text{ eV}$).^{14b,c} Upon the coadsorption of CO and O_2 , the two molecules can come closer to each other while the O–O bond length is elongated. After crossing a relatively low energy barrier of 0.35 eV (TS1 in Figure 3), the two molecular species arrive at a metastable intermediate state, characterized by $\text{O}-\text{C}-\text{O}-\text{O}$ with the O–O bond length being 1.432\AA . The structure of this intermediate is very similar to that on small-sized gold clusters, as reported previously.^{14,20,52} In the next step, the O–O bond length is further elongated and the molecular species reach the second transition state (TS2) with an energy barrier of 0.55 eV . After crossing this barrier, a CO_2 is formed and subsequently desorbed, while the remaining species become an $\text{O}-\text{Au@Cu}_{12}\text{@Au}_{42}^-$ complex. Lastly, after another CO molecule is adsorbed adjacent to the atomic O, the second

CO_2 molecule is formed through a barrierless reaction to complete one catalytic cycle.

The neutral cluster $\text{Au}@\text{Cu}_{12}@\text{Au}_{42}$ exhibits very similar catalytic behavior as the anion counterpart, as shown in Figure 4. The reaction barriers associated with TS1 and TS2 are 0.61 and 0.23 eV, respectively. The TS1 barrier is slightly higher than that for the anion cluster, whereas the TS2 barrier is slightly lower. It should be noted that the catalytic activities of the neutral cluster $\text{Au}@\text{Cu}_{12}@\text{Au}_{42}$ are comparable to those of small-sized neutral gold clusters (for example, Au_{10} ^{14b,c}) and much higher than those of the gold $\text{Au}(211)$ surface.^{52a} Hence, both the anion and neutral crown gold clusters are potentially capable of catalyzing the CO oxidation below the room temperature.

On the basis of the second benchmark reaction, Patil et al. reported highly active (and selective) gold nanoparticles for catalyzing the styrene epoxidation.⁵⁴ $\text{Au}(111)$ surface was also shown to be an effective catalyst for the styrene epoxidation based on the temperature programmed reaction spectroscopy measurement⁵⁴ as well as DFT calculations.^{55,56} A simplified model for the ethylene epoxidation was proposed by Torres and Illas.⁵⁷ Here, the calculated reaction pathways for the selective oxidation of styrene on the active site, namely, a Au_6 triangle on the anion or neutral cluster $I_h\text{-Au}@\text{Cu}_{12}@\text{Au}_{42}$, are shown in Figures 5 and 6, respectively. Both anion and neutral clusters show similar catalytic activities toward the styrene oxidation. On both reaction pathways, the initial step to reach the peroxide state (Figure 5 and Figure 6, a) is slightly endothermic. However, the peroxide state associated with the anion cluster is slightly more stable than that associated with the neutral cluster (anion, 0.31 eV; neutral, 0.44 eV). The energy barrier to dissociate O_2 on both clusters is also very close (anion, 1.61 eV; neutral, 1.67 eV). This relatively high barrier indicates that an excessive electron on $I_h\text{-Au}@\text{Cu}_{12}@\text{Au}_{42}$ hardly affects O_2 activation. Once O_2 is dissociated on the clusters, the styrene can be strongly adsorbed near the preadsorbed atomic O, with adsorption energy of -1.16 eV for the anion and -1.33 eV for the neutral crown-gold cluster. Subsequently, the atomic O can attack C_α of the styrene, followed by crossing an energy barrier to form an oxametallacycle intermediate (OMME) (0.71 eV for anion; 0.77 eV for neutral). This OMME intermediate has been identified in several previous DFT studies of similar reaction on the $\text{Au}(111)$ surface.^{56,57} Thereafter, the OMME can further react to form one of the following three products: acetophenone, styrene epoxide, and benzaldehyde. The formation of acetophenone is most likely due to the largest exothermic energy of -2.20 eV for the anion and -2.03 eV for the neutral cluster. The formation of styrene epoxide is less likely due to modest exothermic energy of -0.69 eV for the anion and -0.78 eV for the neutral. The formation of benzaldehyde is the least likely due to the least exothermic energy of -0.05 eV for the anion and -0.22 eV for the neutral. Meanwhile, the reaction barrier to the acetophenone is also the lowest,

~ 0.92 eV for the anion and 0.76 eV for the neutral. The reaction barrier to the styrene epoxide is 1.09 eV for the anion and 1.00 eV for the neutral, while that to the benzaldehyde is the highest, 2.14 eV for the anion and 2.33 eV for the neutral. These results indicate that the acetophenone can be the dominant product at low temperature on both anion and neutral crown-gold clusters. At elevated temperatures, both styrene epoxide and benzaldehyde can be formed. Note that acetophenone was not observed on the $\text{Au}(111)$ surface in previous experiments⁵⁵ but was detected on bare Au_{55} nanocluster.¹⁵ In any case, the reaction barrier to acetophenone formation on $I_h\text{-Au}@\text{Cu}_{12}@\text{Au}_{42}$ is lower than that on $\text{Au}(111)$ surface,⁵⁷ suggesting that the crown-gold cluster possesses higher catalytic activity and selectivity than the $\text{Au}(111)$ surface.

In conclusion, we have predicted that a 55-atom gold alloy cluster $\text{Au}_{45}\text{Cu}_{12}$ possesses a multishell structure with the highest icosahedral symmetry. More interestingly, this geometric magic-number cluster with many low-coordinated Au atoms is an effective catalyst for the CO oxidation, similar to the small-sized Au_{10} cluster. In addition, it shows higher selectivity for styrene oxidation than the bare $\text{Au}(111)$ surface.

Acknowledgment. This work was supported by grants from NSF (DMR-0820521) and the Nebraska Research Initiative, and by the University of Nebraska Holland Computing Center.

Supporting Information Available. Cartesian coordinates and relative energies for 10 lowest-lying $\text{Au}_{45}\text{Cu}_{12}$ isomers, relative energies of Au_{12}^- 2D and 3D isomers, and complete ref 50 are collected. This material is available free of charge via the Internet at <http://pubs.acs.org>.

REFERENCES AND NOTES

- (1) Grabow, L. C.; Mavrikakis, M. *Angew. Chem., Int. Ed.* **2008**, *47*, 7390.
- (2) Hutchings, G. J.; Burst, M.; Schmidbaur, H. *Chem. Soc. Rev.* **2008**, *37*, 1759.
- (3) Daniel, M.-C.; Astruc, D. *Chem. Rev.* **2004**, *104*, 293.
- (4) (a) Pyykkö, P. *Angew. Chem., Int. Ed.* **2004**, *43*, 4412. (b) Pyykkö, P. *Chem. Soc. Rev.* **2008**, *37*, 1967, and references therein.
- (5) Pina, C. D.; Falletta, E.; Prati, L.; Rossi, M. *Chem. Soc. Rev.* **2008**, *37*, 2077, and references therein.
- (6) (a) Pyykkö, P. *Relativistic Theory of Atoms and Molecules*, Springer: Berlin, 2000; Vol. III, pp 108–111. (b) Schwarz, H. *Angew. Chem., Int. Ed.* **2003**, *42*, 4442.
- (7) (a) Haruta, M.; Kobayashi, T.; Samo, H.; Yamada, N. *Chem. Lett.* **1987**, *405*. (b) Haruta, M.; Yamada, N.; Kobayashi, T.; Iijima, S. *Catal. Today* **1989**, *115*, 301. (c) Haruta, M. *Catal. Today* **1997**, *36*, 115. (d) Haruta, M. *Catal. Today* **1997**, *36*, 153. (e) Haruta, M. *Catal. Today* **1997**, *36*, 153. (f) Bond, G. C. *Catal. Today* **2002**, *72*, 5.
- (8) (a) Wesendrup, R.; Hunt, T.; Schwerdtfeger, P. *J. Chem. Phys.* **2000**, *112*, 9356. (b) Häkkinen, H.; Landman, U. *Phys. Rev. B* **2000**, *62*, R2287. (c) Häkkinen, H.; Moseler, M.; Landman, U. *Phys. Rev. Lett.* **2002**, *89*, 033401.
- (9) Hashmi, A. S. K.; Hutchings, G. J. *Angew. Chem., Int. Ed.* **2006**, *45*, 7896, and references therein.
- (10) (a) Chen, M. S.; Goodman, D. W. *Acc. Chem. Res.* **2006**, *39*, 739, and references therein. (b) Chen, M. S.; Goodman, D. W. *Catal. Today* **2006**, *111*, 22, and references therein. (c) Chen, M. S.,

- Goodman, D. W. *Chem. Soc. Rev.* **2008**, *37*, 1860, and references therein.
- (11) Bond, G. C.; Louis, C.; Thompson, D. T. *Catalysis by Gold*; Imperial College Press: London, 2006.
- (12) Herzing, A. A.; Kiely, C. J.; Carley, A. F.; Landon, P.; Hutchings, G. J. *Science* **2008**, *321*, 1331.
- (13) Chen, M. S.; Goodman, D. W. *Science* **2004**, *306*, 252.
- (14) (a) Sanchez, A.; Abbet, S.; Heiz, U.; Schneider, W.-D.; Häkkinen, H.; Barnett, R. W.; Landman, U. *J. Phys. Chem. A* **1999**, *103*, 9573. (b) Lopez, N.; Norskov, J. K. *J. Am. Chem. Soc.* **2002**, *124*, 11262. (c) Janssens, T. V. W.; Clausen, B. S.; Hvilsted, B.; Falsig, H.; Christensen, C. H.; Bligaard, T.; Norskov, J. K. *Top. Catal.* **2007**, *44*, 15. (d) Remediakis, I. N.; Lopez, N.; Norskov, J. K. *Angew. Chem., Int. Ed.* **2005**, *44*, 1824. (e) Yoon, B.; Häkkinen, H.; Landman, U.; Worz, A. S.; Antonietti, J. M.; Abbet, S.; Judai, K.; Heiz, U. *Science* **2005**, *307*, 403.
- (15) Turner, M.; Golovko, V. B.; Vaughan, O. P. H.; Abdulkin, P.; Berenguer-Murcia, A.; Tikhov, M. S.; Johnson, B. F. G.; Lambert, R. M. *Nature* **2008**, *454*, 981.
- (16) Schwerdtfeger, P. *Angew. Chem., Int. Ed.* **2003**, *42*, 1892.
- (17) Pykkö, P.; Runeberg, N. *Angew. Chem., Int. Ed.* **2002**, *41*, 2174.
- (18) Li, X.; Kiran, B.; Li, J.; Zhai, H.-J.; Wang, L. S. *Angew. Chem., Int. Ed.* **2002**, *41*, 4786.
- (19) Zhai, H.-J.; Li, J.; Wang, L. S. *J. Chem. Phys.* **2004**, *121*, 8369.
- (20) Molina, L. M.; Hammer, B. *J. Catal.* **2005**, *233*, 399.
- (21) Walter, M.; Häkkinen, H. *Phys. Chem. Chem. Phys.* **2006**, *8*, 5407.
- (22) (a) Gao, Y.; Bulusu, S.; Zeng, X. C. *J. Am. Chem. Soc.* **2005**, *127*, 15680. (b) Gao, Y.; Bulusu, S.; Zeng, X. C. *ChemPhysChem* **2006**, *7*, 2245.
- (23) Gao, Y.; Shao, N.; Bulusu, S.; Zeng, X. C. *J. Phys. Chem. C* **2008**, *112*, 8234.
- (24) Zorriastain, S.; Joshi, K.; Kanhere, D. G. *J. Chem. Phys.* **2008**, *128*, 184314.
- (25) Ferrando, R.; Fortunelli, A.; Rossi, G. *Phys. Rev. B* **2005**, *72*, 085449.
- (26) (a) Wang, L. M.; Bulusu, S.; Zhai, H.-J.; Zeng, X. C.; Wang, L. S. *Angew. Chem., Int. Ed.* **2007**, *46*, 2915. (b) Wang, L. M.; Pal, R.; Huang, W.; Zeng, X. C. *J. Chem. Phys.* **2009**, *130*, 051101. (c) Wang, L. M.; Bai, J.; Lechtken, A.; Huang, W.; Schooss, D.; Kappes, M. M.; Zeng, X. C.; Wang, L. S. *Phys. Rev. B* **2009**, *79*, 033413.
- (27) Chang, C. M.; Cheng, C.; Wei, C. M. *J. Chem. Phys.* **2008**, *128*, 124710.
- (28) Cheng, D.; Huang, S.; Wang, W. *Eur. Phys. J. D* **2006**, *39*, 41.
- (29) Cheng, D.; Huang, S.; Wang, W. *Phys. Rev. B* **2006**, *74*, 064117.
- (30) Häkkinen, H.; Moseler, M.; Kostko, O.; Morgner, N.; Hoffmann, M. A.; von Issendorff, B. *Phys. Rev. Lett.* **2004**, *93*, 093401.
- (31) Huang, W.; Ji, M.; Dong, C.-D.; Wang, L.-M.; Gong, X. G.; Wang, L. S. *ACS Nano* **2008**, *2*, 897.
- (32) Xing, X.; Danell, R. M.; Garzón, I. L.; Michaelian, K.; Blom, M. N.; Burns, M. M.; Parks, J. H. *Phys. Rev. B* **2005**, *72*, 081405.
- (33) Jennison, D. R.; Schultz, P. A.; Sears, M. P. *J. Chem. Phys.* **1997**, *106*, 1856.
- (34) Wang, J. L.; Bai, J.; Jellinek, J.; Zeng, X. C. *J. Am. Chem. Soc.* **2007**, *129*, 4110.
- (35) Gao, Y.; Shao, N.; Zeng, X. C. *J. Chem. Phys.* **2008**, *129*, 084703.
- (36) Perdew, J. P.; Burke, K.; Ernzerhof, M. *Phys. Rev. Lett.* **1996**, *77*, 3865.
- (37) (a) Delley, B. *J. Chem. Phys.* **1990**, *92*, 508. (b) Delley, B. *J. Chem. Phys.* **2000**, *113*, 7756.
- (38) (a) Henkelman, G.; Uberuaga, B. P.; Jonsson, H. *J. Chem. Phys.* **2000**, *113*, 9901. (b) Henkelman, G.; Jonsson, H. *J. Chem. Phys.* **2000**, *113*, 9978.
- (39) Wales, D. J.; Scheraga, H. A. *Science* **1999**, *285*, 1368.
- (40) Yoo, S. H.; Zeng, X. C. *Angew. Chem., Int. Ed.* **2005**, *44*, 1491.
- (41) Keal, T. W.; Tozer, D. J. *J. Chem. Phys.* **2003**, *119*, 3015.
- (42) (a) Aikens, C. M. *J. Phys. Chem. A* **2009**, *113*, 10811. (b) Aikens, C. M. *J. Phys. Chem. C* **2008**, *112*, 19797.
- (43) (a) Furche, F.; Ahlrichs, R.; Weis, P.; Jacob, C.; Gilb, S.; Bierweiler, T.; Kappes, M. *J. Chem. Phys.* **2002**, *117*, 6982. (b) Häkkinen, H.; Yoon, B.; Landman, U.; Li, X.; Zhai, H.-J.; Wang, L. S. *J. Phys. Chem. A* **2003**, *107*, 6168. (c) Xing, X.; Yoon, B.; Landman, U.; Parks, J. H. *Phys. Rev. B* **2006**, *74*, 165423.
- (44) Johansson, M. P.; Lechtken, A.; Schooss, D.; Kappes, M.; Furche, P. *Phys. Rev. A* **2008**, *77*, 053202.
- (45) (a) Ferrighi, L.; Hammer, B.; Madsen, G. K. H. *J. Am. Chem. Soc.* **2009**, *131*, 10605. (b) Mantina, M.; Valero, R.; Truhlar, D. G. *J. Chem. Phys.* **2009**, *131*, 064706.
- (46) te Velde, G.; Bickelhaupt, F. M.; Baerends, E. J.; Fonseca Guerra, C.; van Gisbergen, S. J. A.; Snijders, J. G.; Ziegler, T. *J. Comput. Chem.* **2001**, *22*, 931.
- (47) Assadollahzadeh, B.; Bunker, P. R.; Schwerdtfeger, P. *Chem. Phys. Lett.* **2008**, *451*, 262.
- (48) Itoh, M.; Kumar, V.; Adscharis, T.; Kawazoe, Y. *J. Chem. Phys.* **2009**, *131*, 174510.
- (49) Li, J.; Li, X.; Zhai, H.-J.; Wang, L. S. *Science* **2003**, *299*, 864.
- (50) Frisch, M. J. *Gaussian 03*, revision E.01; Gaussian, Inc.: Wallingford, CT, 2004.
- (51) Periyasamy, G.; Remacle, F. *Nano Lett.* **2009**, *9*, 3007.
- (52) (a) Liu, Z.-P.; Hu, P.; Alavi, A. *J. Am. Chem. Soc.* **2002**, *124*, 14770. (b) Liu, Z.-P.; Gong, X.-Q.; Kohanoff, J.; Sanchez, C.; Hu, P. *Phys. Rev. Lett.* **2003**, *91*, 266102. (c) Liu, L. M.; McAllister, B.; Ye, H. Q.; Hu, P. *J. Am. Chem. Soc.* **2006**, *128*, 4017.
- (53) Lemire, C.; Meyer, R.; Shaikhutdinov, S.; Freund, H.-J. *Angew. Chem., Int. Ed.* **2004**, *43*, 118.
- (54) (a) Patil, N. S.; Upadhye, B. S.; Jana, P.; Sonawane, R. S.; Bhargava, S. K.; Choudhary, V. R. *Catal. Lett.* **2004**, *94*, 89. (b) Patil, N. S.; Upadhye, B. S.; Jana, P.; Bharagava, S. K.; Choudhary, V. R. *J. Catal.* **2004**, *223*, 236. (c) Patil, N. S.; Upadhye, B. S.; Jana, P.; Bhargava, S. K.; Choudhary, V. R. *Chem. Lett.* **2004**, *33*, 400. (d) Patil, N. S.; Upadhye, B. S.; Jana, P.; Bhargava, S. K.; Choudhary, V. R. *Appl. Catal., A* **2004**, *275*, 87.
- (55) Deng, X.; Friend, C. M. *J. Am. Chem. Soc.* **2005**, *127*, 17178.
- (56) Xue, L.-Q.; Pang, X.-Y.; Wang, G.-C. *J. Comput. Chem.* **2009**, *30*, 438.
- (57) Torres, D.; Illas, F. *J. Phys. Chem. B* **2006**, *110*, 13310.